Ukrainian Journal of Physical Optics
ISSUE 4
2026

PLASMONIC SILVER NANOPARTICLE LAYERS ON TRANSPARENT CONDUCTIVE SUBSTRATES: DROP-DEPOSITION OF PHOTOMODIFIED COLLOIDS VERSUS LASER-INDUCED IN SITU SYNTHESIS

T. BULAVINETS [1,†], Y. KACHURAK [1], M. SHEPIDA [2], M. LAPINSKI [3], A. LEPEK [3], I. HELZHYNSKYY [1], KH. IVANIUK [1], P. STAKHIRA [1], AND I. YAREMCHUK [1,‡]

[1] Lviv Polytechnic National University, Department of Electronic Engineering, 12 S. Bandery str., Ukraine
[2] Lviv Polytechnic National University, Department of Occupational Safety and Human Life, 12 S. Bandery str., Ukraine
[3] Institute of Nanotechnology and Materials Engineering, Gdansk University of Technology, Advanced Materials Center, 11/12 Gabriela Narutowicza, 80-233 Gdańsk, Poland
[†,‡] Corresponding authors: tetiana.o.bulavinets@lpnu.ua, iryna.y.yaremchuk@lpnu.ua

Received: 12.10.2026

Abstract. We implemented and compared two methods for fabricating plasmonic silver nanoparticle (AgNP) layers on ITO/CuI substrates to determine how the fabrication process affects the layer's morphology and optical properties. First, a colloidal AgNP dispersion is photochemically modified under LED illumination at selected wavelengths. The modified particles are then transferred onto the substrate by drop-depositing. The second method uses laser-assisted photoreduction of silver ions to enable the direct, in situ growth of Ag NPs on the substrate surface. Irradiating a citrate-stabilized colloid of spherical AgNPs with green and red LEDs produces additional plasmon bands at 584 and 975 nm, as well as at 710 and 1050 nm. Depositing drop-modified colloids onto ITO/CuI substrates results in coatings with different morphologies. Coatings with large particles organized into chain-like and network-like aggregates and coatings of small, triangular particles were created. Using laser-induced synthesis to create AgNPs directly on the ITO/CuI surface yields a continuous, uniform layer of anisotropic, platelet-like nanostructures. Rather than colloid pretreatment alone, the deposition route was found to determine the layer architecture, with in situ laser-induced synthesis producing the densest and most uniform layers. The ability to shift the plasmon resonance into the near-infrared range and form dense, uniform plasmonic layers on transparent conductive substrates makes the laser-induced synthesis method promising for enhancing the local electromagnetic field.

Keywords: silver nanoparticles, photomodified colloids, absorption, substrate
UDC: 53.072; 621.38; 621.396
DOI: 10.3116/16091833/Ukr.J.Phys.Opt.2026.04178
This work is licensed under the Creative Commons Attribution International

1. Introduction

The silver nanoparticles (AgNPs) are among the most efficient plasmonic materials for optoelectronics. They are distinguished by several beneficial characteristics, including enhanced electrical [1-3], thermal [4-6], and optical conductivity [7-10]. These properties make them valuable in fields such as catalysis [11, 12], imaging [13–15], electronics [16–18], and optoelectronics [19–21]. Compared to bulk silver, AgNPs have significantly superior physicochemical properties due to changes in their shape and crystallite size. Their increased surface area improves their physical, chemical, and electromagnetic properties, making them ideal for use in micro- and optoelectronic nanodevices [22-24]. The effectiveness of AgNP-based elements depends on their size, shape [25, 26], aggregation state [27,28], surface density, crystallinity, and the distance between the nanoparticles (NPs)

[29-31]. Minor changes in NP morphology can shift plasmonic resonance [32, 33], modify electromagnetic coupling, and significantly affect resonance-spectrum intensity [34, 35]. The shape of NPs is particularly important because anisotropic particles concentrate electromagnetic fields more effectively than spherical particles do [36-38]. Triangular nanoprisms, nanoplates, nanostars, and other polyhedral structures have sharp edges and corners that can act as field-concentrating points [39, 40]. While such features may increase local enhancement, they do not automatically guarantee better analytical performance. The stability and long-term performance of AgNPs in electrical and optoelectronic systems are limited by their unique properties [41]. Research should be focused on increasing the stability and reliability of AgNPs in optoelectronic devices.

Therefore, researchers are paying close attention to various methods for synthesizing silver nanoparticles and their wide range of applications. In particular, AgNPs of various sizes and shapes have been obtained by reducing silver nitrate with sodium borohydride in the presence of polyvinylpyrrolidone and sodium citrate [42, 43]. It has been demonstrated that the morphology and size of the particles can be controlled by adjusting the type and concentration of the reagents, as well as the reaction conditions [44]. Furthermore, it has been demonstrated that colloidal methods produce stable particles that are ideal for surface-enhanced Raman spectroscopy (SERS), optoelectronics, catalysis, and biological imaging [45, 46].

Methods for depositing nanoparticles onto solid substrates are key to transitioning from colloidal systems to functional optical and optoelectronic elements [47]. The choice of deposition method directly affects nanoparticle size, shape, and surface distribution. Consequently, it also affects the position and intensity of the localized surface plasmon resonance. For example, a comparison of the electroless deposition, electrodeposition, and spray pyrolysis of silver on silicon substrates revealed that these methods produce particles with different morphologies and optical responses [48]. Meanwhile, nanoparticles formed by annealing ultrathin silver films can significantly reduce silicon reflectance across a broad spectral range, which is important for photovoltaics [49, 50]. Controlled deposition of silver nanoparticles can also enhance the optical and electrical properties of transparent, conductive substrates such as indium-tin oxide (ITO) [51]. Unconventional approaches, such as visible-light-induced liquid-phase deposition, can enable particles to self-assemble into structures with optimized light-interaction characteristics. This eliminates the need for costly electron-beam lithography [52]. Methods for depositing plasmonic particles onto porous and biological substrates to create colorimetric sensors and SERS-active surfaces are equally promising [53, 54]. Although drop-deposition of colloidal AgNPs is simple and accessible, it often yields non-uniform NP distribution and limited substrate adhesion [55]. In situ growth or laser-assisted formation of NPs directly on a solid substrate can improve contact between the nanoparticles and the substrate, increase surface coverage, and more reproducibly form networks of “hot spots” [56, 57]. Recent studies of photochemical, laser-induced, lithographic, and self-assembled substrates demonstrate that achieving high sensitivity and reproducibility requires controlled nanostructural organization [58, 59]. Thus, depositing nanoparticles onto different substrates is not only a technological step, but also an effective tool for controlling the optical properties of future devices. Despite growing attention to the substrate's role, the deposition step is often treated as routine. Systematic comparative studies relating the deposition route to the resulting coating morphology, uniformity, and optical response remain scarce. This gap is especially important for applications that depend on dense, uniform plasmonic layers on transparent, conductive

substrates. In these applications, the spectral position of the plasmon resonance and the surface density of electromagnetic hot spots both determine device performance.

This work aims to establish how the fabrication process influences the morphology and optical properties of AgNP layers on ITO/CuI substrates. To this end, we adopted two fundamentally different methods for this substrate and compared them using identical characterization methods. In the first method, colloidal AgNPs undergo photochemical transformation by LED irradiation at specific wavelengths, shifting their plasmon resonance into the NIR range. We then drop-deposit the AgNPs onto the substrate. The second method grows AgNPs directly on the substrate surface using laser-induced photoreduction. We demonstrate that the deposition method largely determines the final layer architecture, rather than colloidal pretreatment alone. We also propose a mechanism linking the observed morphologies to plasmon-induced coalescence within the colloid and capillary assembly during droplet drying. By correlating morphology with optical transmission, we established that in situ laser-induced synthesis is the most effective method of producing dense, uniform plasmonic layers. Finally, we consider the relevance of these structures for SERS sensing and NIR photodetectors.

2. Materials and Methods

2.1. Synthesis of AgNPs

The synthesis of triangular AgNPs occurred in two stages. First, silver ions were reduced from a 4 mM aqueous solution of silver nitrate ($AgNO_3$, SferaSim, 99.8%) using continuous laser radiation at a wavelength of 445 nm (power: 380 mW) in the presence of a 4 mM aqueous solution of trisodium citrate ($Na_3C_6H_5O_7$, SferaSim, 99.5%) as a stabilizing agent. All materials were used as received, without further purification. The Ag_0 synthesis was carried out at room temperature (20°C) with constant stirring, according to the following scheme:

$$AgNO_3 \rightarrow Ag^+ + NO_3^-$$

$$Na_3C_6H_5O_7 \rightarrow 3Na^+ + C_6H_5O_7^{3-}$$

At 20°C, trisodium citrate does not split into separate reducing agents. After light excitation, it directly donates electrons and simultaneously stabilizes the AgNPs. At room temperature, the reaction is slower but more controllable, leading to uniform, stable nanoparticles. Therefore, it follows that:

$$Ag^+ + C_6H_5O_7^{3-} \xrightarrow{\lambda=445nm} Ag^0 + C_6H_5O_7^{ox}$$

The next stage involves photon-controlled growth of NPs with shape formation. The resulting colloid of spherical AgNPs was divided into two separate portions. Each portion was then irradiated for 36 hours using LED radiation at a single wavelength: red at 633 nm with a total power of 170 mW or green at 532 nm with a total power of 150 mW. Uniform irradiation was ensured from all sides and along the entire height of the 1 cm diameter vial containing the colloidal solution. To achieve this, the LEDs were mounted inside a 5 cm diameter cylinder, facing towards the center, where the vial was positioned. Additionally, the heat generated by the LEDs was dissipated to ensure that any observed modifications were

specifically caused by the light. Prolonged LED irradiation causes intense electron oscillations on specific crystallographic faces. Trisodium citrate is partially removed from these faces, revealing active growth sites. Anisotropic growth occurs slowly in the {111} planes [60]. These faces are more stable and form flat prisms. The {100} and {110} planes are less stable. Growth under the influence of light occurs more rapidly here [61]. Consequently, different LED wavelengths produce different growth rates, leading to silver triangle NPs of varying thickness and size.

2.2. Formation of AgNPs-based substrates

The synthesized AgNP colloidal solution was deposited on the substrates by drop deposition. To improve nanoparticle adhesion to the substrate, a thin (~5 nm) CuI film was deposited on ITO glass by thermal vacuum deposition. Then, the surface was treated with UV-ozone for 30 min using a UV-Ozone Cleaner (Ossila, UK). The AgNP dispersion (30 μl) was drop-deposited onto a preheated ITO/CuI substrate (25×15 mm). It was then dried for 10 minutes on a hot plate at 40°C.

2.3. Synthesis of AgNPs directly on the substrate

An alternative approach based on laser-induced in situ growth of AgNPs directly on the substrate surface [62] was employed to promote nanoparticle deposition and surface attachment. In this case, the AgNPs were synthesized directly on the ITO/CuI substrate. To achieve this, the ITO/CuI substrate was immersed in an aqueous solution containing 10 mL of 4 mM $AgNO_3$ and 40 mL of 4 mM $Na_3C_6H_5O_7$, for a 1:4 ratio. A 380 mW, 445 nm continuous laser beam was focused onto a 5×3 mm area of the substrate surface. The synthesis was carried out at room temperature (approximately 20°C) with continuous magnetic stirring at 600 rpm.

2.4. Characterization

We examined the morphology of the synthesized silver nanostructures using microscopic techniques. The formation of the nanostructures and the surface morphology of the samples were observed and analyzed using a FEI Quanta FEG 250 scanning electron microscope (SEM) operating at 20 kV. Additionally, an energy-dispersive X-ray spectrometer (EDS) was used to analyze the elemental composition of the nanostructures. The average size of the NPs was estimated from SEM images by measuring a statistically representative number of NPs in different regions of the surface. We analyzed the absorption spectra of the obtained silver colloids using a UV-Vis Evolution 220 spectrophotometer. Raman spectra were acquired using a confocal Raman spectrometer (XploR PLUS, Horiba Jobin Yvon), which was equipped with a 532-nm excitation laser and a grating monochromator with 1,200 grooves per millimeter. Measurements were performed using a 10x objective. Before measurements, the instrument was calibrated using the characteristic silicon band at 520.7 cm^{-1}. The optical properties of AgNPs were calculated using the discrete dipole approximation (DDA) [63, 64]. This computational technique can model metal nanoparticles of any non-spherical shape with high numerical accuracy. The target particle is represented by an array of many small, polarizable, cubic elements that are solely coupled to one another through dipole–dipole interactions. Each element responds to the local electric field acting on it by developing an induced dipole moment. The resulting polarizations of all the elements are then used to calculate the particle's extinction cross-section. The nanoprism discretization satisfied the DDA validity criterion for total cross sections across the entire studied spectral range. The

measuring 150×10 nm (with a quadrupole band near 620 nm and a dipole band near 970 nm) is similar to that of the green-modified colloid (with peaks at 584 and 975 nm). For larger prisms (230×13 nm), the quadrupole modes shift to 650–800 nm, and the dipole resonance moves beyond 1000 nm. This is consistent with the red-modified colloid spectrum (710 and 1050 nm). Thus, the red shift of the plasmon bands when moving from green to red light reflects an increase in the edge length (and aspect ratio) of the nanoprisms. The experimental bands are broader than the calculated ones. This can be attributed to the size and shape distribution of the colloidal particles, including those with truncated prism corners.

SEM images of coatings obtained by drop-depositing AgNP colloids that were pre-modified by irradiation in the red (Substrate A) and green (Substrate B) spectral ranges onto ITO/CuI substrates are shown in Fig. 2. The different coating morphologies indicate significant differences in the composition and state of the particles in the initial colloids.

Relatively large particles with distinct faceting formed on Substrate A. These particles tend to aggregate into chain-like and network-like structures that extend up to several micrometers. This aggregation pattern results in significant coating non-uniformity. Alongside agglomerates, large areas of the substrate are virtually free of particles. The mean maximum lateral dimension of the particles and their aggregates identified in the SEM images is 225 ± 172 nm, with a median of approximately 175 nm. In contrast, Substrate B's surface is predominantly covered with small, densely and uniformly distributed triangular particles, with occasional compact submicron-sized aggregates. The mean equivalent particle diameter is 53 ± 42 nm, and the mean maximum lateral dimension is 68 ± 62 nm. The median is approximately 45 nm. The mean being significantly higher than the median indicates positive skew in the distribution, driven by a few large aggregates. Substrate A also exhibits a similar, albeit less pronounced, asymmetry.

Fig. 2. SEM images of coatings obtained by drop-depositing AgNP colloids that were pre-modified by irradiation in the red (Substrate A) and green (Substrate B) spectral ranges onto ITO/CuI substrates.

The differences in coating morphology are consistent with the spectral data for the modified colloids (Fig. 1b). The larger wavelength shift of the plasmon bands for the colloid irradiated with red light corresponds to the formation of larger, more anisotropic particles. This aligns with the known dependence of nanoprism size on excitation wavelength. Meanwhile, the dimensions of the faceted particles on Substrate A far exceed the characteristic sizes of the nanoprisms that formed during the photoinduced growth process. This suggests that particle coalescence occurred alongside anisotropic growth as early as the

colloid irradiation stage. Plasmon-induced fusion of nanoprisms has been observed for silver [66]. For gold nanoparticles, morphological transformation has been shown to occur via a hot-hole-driven mechanism dominated by coalescence [67, 68]. The plasmonic properties of noble metals are similar, which suggests that this mechanism may also operate in the Ag system. Plasmonically coupled aggregates may also partially account for the high intensity of the absorption band around 1050 nm.

How the droplet dries is another factor that determines the nature of aggregation. During solvent evaporation, capillary flows arise and transport particles toward the droplet periphery, promoting their local concentration. In the final stage of drying, when the liquid film thickness falls below the particle size, lateral capillary forces emerge between them. The intensity of these forces increases with particle size. Consequently, the large particles of colloid modified by red LED radiation (A) experience stronger capillary and van der Waals attractions. These particles organize into chain-like and network structures. In contrast, the small particles of colloid modified by green LED radiation (B) remain mobile for a longer period of time. They deposit onto the substrate much more uniformly.

Fig. 3 shows the transmission spectra of substrates A and B over 350–1100 nm. The ITO/CuI substrates have AgNPs deposited from colloids A and B, which emit red and green light, respectively. The spectral profile of the bare ITO/CuI substrate matches that of the coated samples, confirming that the substrate governs the overall spectral shape. The AgNP layers further reduce transmittance. In the NIR range, transmittance decreases monotonically for both samples. Because the bare substrate already shows a significant decrease in this range due to free-carrier absorption in ITO, the further reduction in the coated samples is due to the long-wavelength plasmon modes of the anisotropic nanoparticles and their aggregates. Both samples show maximum transmission near 430 nm. The short-wavelength drop-off likely results from interband absorption in CuI, whose absorption edge is around 410 nm. Further along the spectrum, a minimum appears in the range of 540–580 nm, followed by a broad maximum in the range of 640–660 nm. This oscillatory structure likely arises from interference within the ITO layer because the CuI film thickness (5 nm) is insufficient to produce interference fringes in the visible spectrum.

Superimposed on this interference pattern is the plasmon absorption of the silver nanoparticles. This absorption is shifted toward longer wavelengths due to the substrate's high refractive index and the electromagnetic interactions between the particles within the

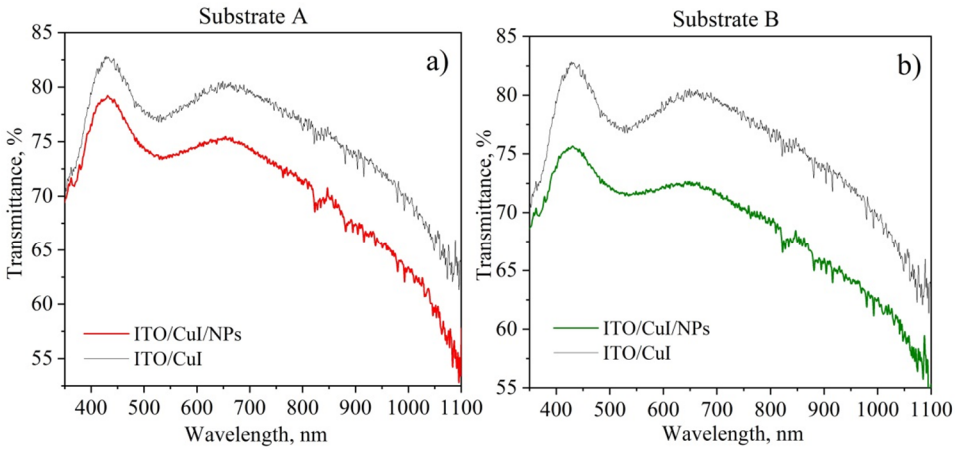

Fig. 3. Experimentally measured optical transmittance spectra of AgNPs-based Substrates A (a) and B (b).

aggregates. In the near-infrared range (700–1,100 nm), transmittance decreases monotonically to 53–55%. This decrease can be attributed to free-carrier absorption in the ITO and the contribution of long-wavelength plasmon modes from anisotropic nanoparticles and their aggregates. A feature appears at the same position in both spectra in the 820–850 nm region and is likely an instrumental artifact associated with switching the spectrophotometer's detector or light source.

Despite their similar shapes, the samples' spectra differ in absolute transmittance. In the visible region, Substrate A has a higher transmittance: approximately 79% at the maximum wavelength of 430 nm and 73-75% in the 550-650 nm range. For Substrate B, these values are approximately 75.6% and 71.5-72.5%, respectively. These results are consistent with those of the SEM analysis. The dense, uniform coverage of Substrate B's surface with small nanoparticles, whose dipole and quadrupole plasmon modes lie within the visible spectrum, results in higher extinction in this region. By contrast, large portions of the substrate surface are free of particles. This reduces the effective surface coverage and, consequently, the transmittance losses in the visible range.

In the NIR, however, the relationship is reversed. At 1100 nm, Substrate A has a transmittance of about 53%, slightly lower than Substrate B at about 55%. This is likely due to large, faceted particles and chain-like aggregates on Substrate A. The plasmon resonance of these particles is shifted toward longer wavelengths due to their increased size and interparticle plasmon coupling. The reduced transmittance may also result from light scattering by large aggregates, whose efficiency increases with aggregate size. Thus, differences in the morphology of nanoparticles obtained from colloids modified by radiation of different wavelengths are evident in their transmission spectra. This is primarily due to a redistribution of extinction between the visible and NIR regions rather than a shift in the position of the main spectral features. The latter is predominantly determined by the substrate.

To enable comparison with coatings obtained by drop-depositing pre-synthesized colloids, we synthesized the AgNPs directly on an ITO/CuI substrate. The sample obtained in this manner is called Substrate C (Fig. 4).

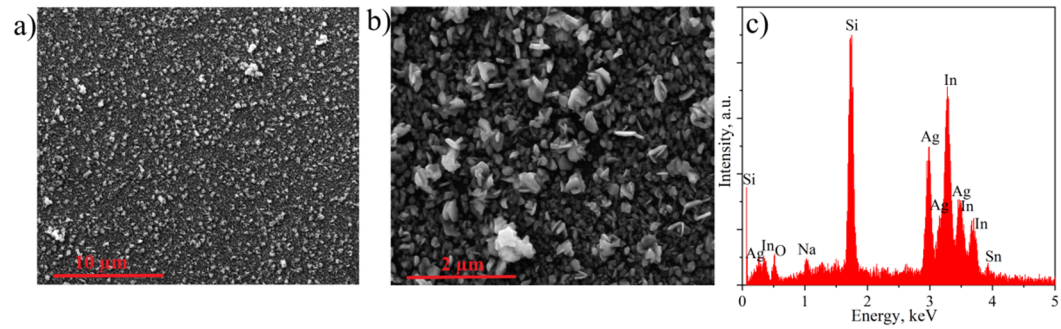

Fig. 4. SEM images of coating obtained by the laser-induced AgNPs formation on the ITO/CuI substrate (a,b) and Energy-dispersive X-ray spectroscopy (EDX) spectra (c) of the AgNPs-modified surface of Substrate C.

An SEM image (Fig. 4a) shows that laser-induced synthesis forms a continuous, dense, uniform layer of silver nanostructures over areas spanning tens of micrometers. The surface has virtually no particle-free regions, and agglomerates 1–2 μm in size occur only sporadically. Fig. 4b reveals that the layer consists of densely packed faceted particles, many of which exhibit a lamellar morphology with distinct edges. Some of the plates are oriented

perpendicular to or at an angle to the substrate surface. In the image, they appear as narrow, elongated strips, which is a characteristic feature of thin nanoplates.

A quantitative analysis of scanning electron microscope (SEM) images revealed that the mean equivalent diameter of the nanostructures on Substrate C is 101 ± 82 nm. The mean maximum lateral dimension is 168 ± 134 nm, with a median of approximately 121 nm. The mean being greater than the median indicates positive skew in the distribution, resulting from the presence of both individual nanoparticles and small aggregates.

In terms of morphology, Substrate C differs significantly from samples that were prepared using the drop-deposition method. Unlike Substrate A, which has a pronounced, chain-like aggregation of large, anisotropic particles and a substantial open surface area, Substrate C has a denser population of smaller, more closely spaced nanostructures that are uniformly distributed across its surface. The particles on Substrate C are larger and more anisotropic than those on Substrate B, and the surface coverage is higher. Thus, in situ particle growth directly on the substrate surface yields significantly higher surface coverage and more uniform coatings than colloid drop deposition.

Energy-dispersive X-ray microanalysis results confirm the formation of AgNPs on the ITO/CuI surface (Fig. 4c). The EDS spectrum shows strong Ag L-series lines between 2.9 and 3.4 keV, which confirms the presence of metallic silver on the surface. The In and Sn signals correspond to the ITO layer. The intense Si line, along with the O and Na signals, originates from the glass substrate because the X-ray generation depth exceeds the coating's total thickness. Residual sodium citrate may also contribute to the Na signal. The spectrum shows no Cu or J lines because the CuI layer is very thin (5 nm). This results in a signal that falls below the method's detection limit against the background of the intense substrate lines.

The transmission spectrum of Substrate C in the range of 350 to 1100 nm is shown in Fig. 5. The overall shape of the spectrum is similar to Substrates A and B, which confirms that the ITO/CuI substrate's optical properties are the dominant contributor to the overall transmission profile. The maximum transmission lies near 425 – 430 nm at approximately 83%. As with Substrates A and B, the short-wavelength drop likely results from interband absorption in CuI. Further along, a minimum is observed in the 520–540 nm region (approximately 77.5%), as well as a broad maximum at 650– 670 nm (approximately 80.5%). These correspond to the ITO interference structure and the plasmonic absorption of the silver nanostructures superimposed on it. Transmission decreases monotonically in the NIR range, reaching approximately 61 – 62% at 1100 nm. As with Substrates A and B, the

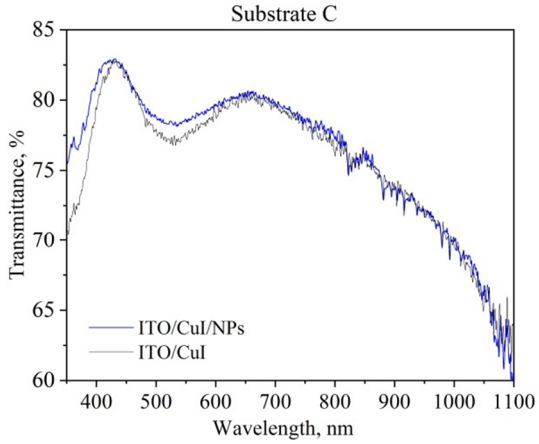

Fig. 5. Experimentally measured optical transmittance spectra of AgNPs-based Substrate C.

feature in the 840 – 850 nm region likely arises from instrumental factors. However, the increased noise level above 900 nm is associated with the spectrophotometer's declining detector sensitivity.

Substrate C exhibits higher transmittance across the entire investigated range than Substrates A and B. The difference is 4 – 7% at the 430 nm peak and 6 – 8% at 1100 nm.

This result is somewhat unexpected, considering the significantly higher surface coverage of nanostructures on Substrate C. One possible explanation is the absence of large aggregates, which characterize Substrate A. This reduces light scattering and yields a smaller average particle size than on Substrate A. At the same time, these differences may partly reflect changes in the substrate itself during laser-induced synthesis in an $AgNO_3$ solution, or variations in the residual organic layer in samples prepared by droplet deposition of colloids. A comparison with the spectrum of the pristine ITO/CuI substrate is necessary to distinguish between these factors.

The performance of the obtained substrates as SERS-active platforms was evaluated by comparing the signal intensity of the model analyte, methylene blue (MB) (Fig. 6). Raman spectra were recorded using a Horiba Aramis UV Raman microscope with 532-nm laser excitation. To compare the signal enhancement provided by different substrates using SERS, we used the same MB solution for all samples and applied it to their surfaces by drop-depositing. This ensured identical conditions for analyte deposition and spectral acquisition. commercially available Ag-based SERS substrate was used as a reference.

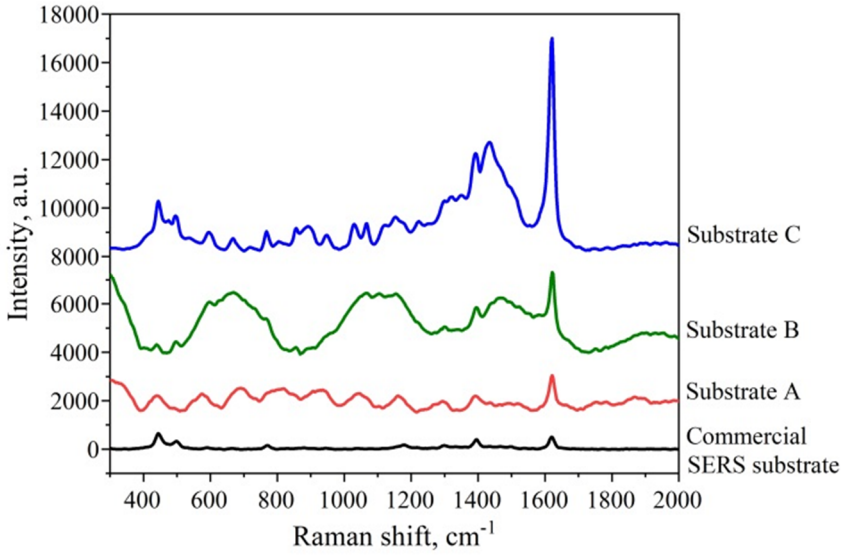

Fig. 6. SERS spectra of methylene blue on Substrates A, B, and C and on a commercial SERS substrate under identical measurement conditions (λ_{exc} = 532 nm; Aramis UV; Horiba). The spectra are vertically offset for clarity.

MS bands [69] were observed on all substrates. The bands appear at the same positions on all substrates. This indicates no significant changes in the analyte's molecular structure during adsorption onto the nanostructure surface. At the same time, the SERS signal intensity varies greatly depending on the substrate type. The intensity of the band at 1624 cm^{-1} for Substrates A and B is about 2-3 and 5-6 times higher than the corresponding value for the commercial substrate, respectively. For Substrate C, the excess is about 15 times higher. The SEM results are consistent with Substrate C's highest efficiency. Dense,

uniform coverage of anisotropic silver nanostructures with clear edges and small interparticle gaps provides a high surface density of hot spots, or regions of local electromagnetic field enhancement. In contrast, Substrate A has a significant amount of particle-free surface area, despite the presence of large anisotropic particles. This reduces the effective number of hot spots in the excitation spot. The intermediate position of Substrate B corresponds to a dense coating formed mainly of small particles.

Significantly, the 532 nm excitation wavelength falls within the spectral region of minimum transmission for all substrates studied (520–580 nm; see Figs. 3 and 5), where plasmonic absorption by silver nanostructures contributes substantially. Thus, these measurement conditions efficiently excite localized surface plasmons, a prerequisite for the electromagnetic mechanism of SERS enhancement.

Notably, red-light photo-induced modification of the colloid forms anisotropic AgNPs that exhibit intense plasmonic bands at 975 and 1050 nm, within the NIR range. These approaches are promising for fabricating plasmonic layers in NIR graphene photodetectors with photogating-based gain and integrated dielectric metasurfaces [70, 71]. Such devices are intended for security and border monitoring systems, where local electromagnetic field enhancement within the detector's operating spectral range increases sensitivity.

4. Conclusions

This work demonstrates that irradiating a citrate colloid of spherical silver nanoparticles with green and red LEDs transforms them into anisotropic triangular nanoprisms. This transformation is evidenced by the appearance of additional plasmon bands, which are attributed to quadrupole and dipole resonances within the prism plane. Exposure to red light shifts the wavelength of these bands to 710 and 1050 nm. Thus, the irradiation wavelength can be used to control the plasmon resonance position, specifically by shifting it into the near-infrared range.

The morphology of the coatings formed by drop-depositing modified colloids onto ITO/CuI substrates depends significantly on the modification conditions. A colloid irradiated with red light forms a heterogeneous coating of large, faceted particles and chain-like or network-like aggregates. In contrast, a colloid irradiated with green light yields a dense, uniform coating of small, triangular particles. The transmission spectra of the coatings are primarily determined by interference within the ITO layer. Differences in particle morphology, by contrast, manifest as a redistribution of extinction between the visible and near-infrared regions. The laser-induced synthesis of AgNPs on the ITO/CuI surface creates a continuous, uniform layer of anisotropic lamellar nanostructures while maintaining the substrate's high optical transmission. The controllable shift of plasmon resonance into the NIR, the formation of dense, uniform plasmonic layers on transparent and conductive substrates, and the effective enhancement of the local electromagnetic field define the application areas for the proposed approaches.

Funding. This research was supported by the Ministry of Education and Science of Ukraine under the projects № 0126U004018 and 0124U000823, and the Polish National Agency for Academic Exchange (NAWA).

Conflicts of interest. The authors declare no conflicts of interest. The authors declare that they have no known competing financial interests or personal relationships that could have appeared to influence the work reported in this paper.

Authors' contribution. Conceptualization, B.T. and Y.I.; methodology, S.M. and I.Kh.; formal analysis, Y.I. and I.Kh.; investigation, B.T., L.M., L.A.; numerical modeling, K.Y. and H.I.; validation, S.P.; writing–original paper, B.T.; writing–review & editing, Y.I. and S.P. All authors have read and agreed to the published version of the manuscript.

References

1. Chaudhuri, B., Ghosh, S., & Mondal, B. N. (2025). Green synthesized silver nanoparticles and PVA composite films showing enhanced protein adsorption, conductivity and dielectric permittivity: Suitable candidate for electronic and biomedical applications. *Materials Science and Engineering: B*, *317*, 118221.
2. Wang, M., Cheng, L., Hou, J., Chen, S., Jiang, L., & Zhou, Y. (2026). Fabrication of aramid nanofiber/silver nanoparticles composite aerogels for enhanced electromagnetic interference shielding. *Chemical Engineering Journal*, 177122.
3. He, X., Deng, G., Xu, H., Zhang, Z., & Mao, H. (2025). Enhanced electrical conductivity and antibacterial properties of bacterial cellulose composite membrane decorated with hydroxypropyl-β-cyclodextrin/magnetic particle/alpha-lipoic acid/nano silver. *International Journal of Biological Macromolecules*, *300*, 140281.
4. Han, G., Cheng, H., He, C., Feng, Y., & Liu, C. (2022). Silver nanoparticles bridging segregated hexagonal boron nitride networks for enhancing the thermal conductivity of polystyrene composites. *Composites Communications*, *34*, 101267.
5. Van Trinh, P., Ngoc Anh, N., Thi Phuong, M., Tu, N. V., Hau, T. V., Tuan, D., ... & Chuc, N. V. (2026). Experimental study on the thermal conductivity of graphene–carbon nanotube–silver nanoparticle ternary hybrid nanofluids. *RSC advances*, *16*(4), 3753-3764.
6. Zhu, J., Jiang, M., Lin, B., Zhang, X., & Sun, Y. (2025). Screen-printable liquid metal–silver core–shell particles: high thermal stability, electrical conductivity, and low silver content. *Materials Letters*, 139924.
7. Navya, N., Sumantha, H. S., & Suresha, B. L. (2025). Improvement in electro-optical and dielectric properties of silver nanoparticles dispersed in a nematic liquid crystal. *Solid State Communications*, *404*, 116068.
8. Sengwa, R. J., Saraswat, M., & Charan, C. P. (2025). Enhanced optical absorption and promising properties by in situ grown plasmonic silver nanoparticles in TiO2, BaTiO3, and SnO2 semiconductor oxide nanomaterials dispersed ethylene glycol based hybrid nanofluids. *Next Research*, 100625.
9. Verma, H., Lal, A., Singh, P. K., Pandey, M. B., Dabrowski, R., & Dhar, R. (2024). Silver nanoparticles induced enhanced stability, dielectric anisotropy, and electro-optical parameters of a nematic liquid crystalline material 4-(trans-4-n-hexylcyclohexyl) isothiocyanatobenzene. *Journal of Molecular Liquids*, *400*, 124503.
10. Wang, K. S., Lan, H. T., Wu, C. H., Chen, Y. C., Lin, Y. J., Sung, T. J., ... & Liu, T. Y. (2024). Electrochemical polymerization of PEDOT: PSS with graphene oxide and silver nanoparticles for antibacterial coating and SERS detection. *Surface and Coatings Technology*, *485*, 130889.
11. Sadaf, S., Bibi, F., Irfan, A., Begum, R., & Farooqi, Z. H. (2026). Advances in carbohydrate polymer-stabilized silver nanoparticles for catalysis. *Carbohydrate Polymers*, 125773.
12. Ahmad, A., Roy, P. G., Zhou, S., Irfan, A., Kanwal, F., Begum, R., & Farooqi, Z. H. (2023). Fabrication of silver nanoparticles within chitosan based microgels for catalysis. *International journal of biological macromolecules*, *240*, 124401.
13. Zhang, R., Dias, M., Li, Y., Rütten, S., Kiessling, F., Lammers, T., & Pallares, R. M. (2025). Structural engineering of silver nanoparticles for enhanced photoacoustic imaging. *Nanoscale advances*, *7*(19), 6110-6119.
14. Berasarte, I., Bordagaray, A., Garcia-Arrona, R., Ostra, M., & Vidal, M. (2025). Silver nanoparticles for the colorimetric determination of electrolytes by UV–vis spectrophotometry and digital image analysis. *Sensing and Bio-Sensing Research*, *49*, 100831.
15. Song, D. H., Song, C. W., Chung, J., Jang, E. H., Kim, H., Hur, Y., ... & Chang, J. B. (2023). In situ silver nanoparticle development for molecular-specific biological imaging via highly accessible microscopies. *Nanoscale Advances*, *5*(6), 1636-1650.
16. Chandak, V. S., & Nagime, P. V. (2025). Synthesis, characterization and applications of silver nanoparticles (Ag-NPs) in the field of electronics and optoelectronics device-a review. *Hybrid Advances*, *8*, 100389.
17. Yang, Y., Bai, N., Cao, T., Zhang, X., Gao, Y., Zhang, J., ... & Huang, J. (2022). Numerical and experimental investigations on intense pulsed light sintering of silver nanoparticle inks for printed electronics. *International Journal of Thermal Sciences*, *176*, 107507.
18. Wang, X., Yang, X., Wang, X., & Ran, R. (2021). Silver nanoparticles prepared by solid-state redox route from HEC for conductive, long-term durable and recycling artificial soft electronics. *Polymer*, *229*, 123974.
19. Gök, G., Yeşilyurt, F., & Deniz, A. R. (2026). Enhanced Optoelectronic and Antibacterial Performance of a Bio-Based Cellulose–Silver Nanocomposite Interlayer for Silicon Photodiodes. *Journal of Alloys and Compounds Communications*, 100211.

20. Amghar, M., Abdellaoui, B., Hajlaoui, M. E., Bejar, M., Oueslati, A., & Dhahri, E. (2026). Effect of 10% Ag doping on the structural, optical, and electrical properties of $ZnAl_2O_4$ nanoparticles for optoelectronic studies. *Journal of Alloys and Compounds*, 191107.
21. Dortaj, H., Matloub, S., & Baghban, H. (2026). Advancements in emerging materials for visible-to-infrared photodetectors: A comprehensive review. *Infrared Physics & Technology*, 106800.
22. Chen, X., Qin, F., Ren, Y., Huang, J., Liang, L., & Zeng, C. (2026). Plasmonic nanodevices: Materials, micro-nano structures and performance. *Advances in Colloid and Interface Science*, 103851.
23. Khalif, A. A., Salma, U., Zonayed, M. D., Rimon, M. I. H., Mimona, M. A., & Mobarak, M. H. (2025). Advances and significances of organic nanomaterials in optoelectronic applications. *Nano-Structures & Nano-Objects*, *41*, 101420.
24. Wu, Y., Zhang, P., Feng, T., Zhu, H., Liu, Y., & Yuan, X. (2026). Metal nanocluster-based nanocomposites: Rational design, interfacial synergy, and emerging functions. *Coordination Chemistry Reviews*, *561*, 217923.
25. Prajapati, S., Kumar, A., & Singh, R. (2026). Environmental applications of silver nanoparticles: state-of-the-art review and emerging trends. *Beilstein Journal of Nanotechnology*, *17*(1), 697-736.
26. Meher, A., Tandi, A., Moharana, S., Chakroborty, S., Mohapatra, S. S., Mondal, A., ... & Chandra, P. (2024). Silver nanoparticle for biomedical applications: A review. *Hybrid Advances*, *6*, 100184.
27. Oliveira, M. J. D. S., Ruiz, G. C. M., Rubira, R. J. G., Sanchez-Cortes, S., Constantino, C. J. L., & Furini, L. N. (2025). Consequences of surface composition and aggregation conditions of Ag nanoparticles on surface-enhanced Raman scattering (SERS) of pesticides. *Chemosensors*, *13*(1), 13.
28. Liu, J., Cao, T., Li, B., Zhang, X., Duan, L., Zhang, T., & Chen, W. (2025). Non-monotonic effects of sulfidation on the aggregation behavior of surface-coated silver nanoparticles. *Journal of Environmental Sciences*.
29. Hossain, M. K., Drmosh, Q. A., & Arifuzzaman, M. (2022). Silver nanoparticles, nanoneedles and nanorings: impact of electromagnetic near-field on surface-enhanced Raman scattering. *Physical Chemistry Chemical Physics*, *24*(15), 8787-8799.
30. Pham, N. B. T., Tran, Q. V., Luong, H. N., Nguyen, T. T., Bui, T. T. T., Duy, L. T., ... & Tran, C. K. (2024). SERS behaviors of multi-shape silver nanoparticles on Si substrate–an insight from both experimental and theoretical approaches. *Colloids and Surfaces A: Physicochemical and Engineering Aspects*, *684*, 133091.
31. Sherpa, L., Nimmala, A., Rao, S. N., Khan, S. A., Pathak, A. P., Tripathi, A., & Tiwari, A. (2024). Refining shape and size of silver nanoparticles using ion irradiation for enhanced and homogeneous SERS activity. *Discover Nano*, *19*(1), 51.
32. Tahir, D., Ramlan, N. M., Isnaeni, I., Afiff, A. F., & Suliyanti, M. M. (2026). Role of substrates and silver nanoparticles in enhancing Raman signal via electromagnetic and chemical enhancement mechanisms. *Materials Chemistry and Physics*, 132475.
33. Bulavinets, T., Yaremchuk, I., & Bobitski, Y. (2017, February). Spectral properties of TiO 2-Ag nanoshells with different shapes for biomedical applications. In *2017 14th International Conference The Experience of Designing and Application of CAD Systems in Microelectronics (CADSM)* (pp. 441-444). IEEE.
34. Bavali, A., Afshar, M., & Rahmatpanahi, A. (2025). Surface Plasmon-Enhanced fluorescence of Spirulina microalgae via triangular silver nanoparticles. *Spectrochimica Acta Part A: Molecular and Biomolecular Spectroscopy*, *340*, 126348.
35. Schiavi, S., Taglietti, A., Magni, A., Galinetto, P., & Albini, B. (2025). Increasing SERS performance of silver nanoparticles with nanometric coating of polydopamine: A novel approach for methylene blue detection. *Applied Surface Science*, *687*, 162223.
36. Bulavinets, T., Grokhotov, V., Helzhynskyy, I., Bulavinets, B., Stakhira, P., & Yaremchuk, I. (2026). Morphological Engineering of Plasmonic Nanostructures: Simulation of Optical Response for Nanoparticles with Basic Geometries. *Ukrainian Journal of Physical Optics*, *27*(1), 01054-01069.
37. Ilin, O., Smachylo, Y., Mysiuk, Y., Bulavinets, T., Fitio, V., & Yaremchuk, I. (2024, May). Silver Ellipsoidal Nanoparticles for Surface Enhanced Raman Scattering Applications. In *2024 IEEE 42nd International Conference on Electronics and Nanotechnology (ELNANO)* (pp. 219-222). IEEE.
38. Alzahrani, R. A., Alhaddad, F. G., Alshammari, E. O., Alsowaileh, F. S., Alghamdi, M. D., Modwi, A., ... & Alqarni, L. S. (2025). Silver nanoparticles in gas sensing: A comprehensive review of synthesis, mechanisms, performance metrics, and emerging applications. *Journal of Science: Advanced Materials and Devices*, 100964.
39. Anh, C. T., Cao, D. T., & Ngan, L. T. Q. (2025). Preparation of Colloidal Silver Triangular Nanoplates and Their Application in SERS Detection of Trace Levels of Antibiotic Enrofloxacin. *Colloids and Interfaces*, *9*(3), 31.
40. Urbina, I., Herrera, L. J. M., Etcheverry, M. E., Villa, C., Sepúlveda, R. D. M., Garavaglia, L., ... & Tebaldi, M. C. (2025). Shape modification of silver nano triangles under light irradiation. *Photonics and Nanostructures-Fundamentals and Applications*, 101470.

41. Hosny, S., Gaber, G. A., Ragab, M. S., Ragheb, M. A., Anter, M., & Mohamed, L. Z. (2025). A comprehensive review of silver nanoparticles (AgNPs): synthesis strategies, toxicity concerns, biomedical applications, AI-driven advancements, challenges, and future perspectives. *Arabian Journal for Science and Engineering*, 1-48.
42. Zannotti, M., Vicomandi, V., Rossi, A., Minicucci, M., Ferraro, S., Petetta, L., & Giovannetti, R. (2020). Tuning of hydrogen peroxide etching during the synthesis of silver nanoparticles. An application of triangular nanoplates as plasmon sensors for Hg2+ in aqueous solution. *Journal of Molecular Liquids*, *309*, 113238.
43. Dawadi, S., Katuwal, S., Gupta, A., Lamichhane, U., Thapa, R., Jaisi, S., ... & Parajuli, N. (2021). Current research on silver nanoparticles: synthesis, characterization, and applications. *Journal of nanomaterials*, *2021*(1), 6687290.
44. Sau, T. K., & Rogach, A. L. (2010). Nonspherical noble metal nanoparticles: colloid-chemical synthesis and morphology control. *Advanced materials*, *22*(16), 1781-1804.
45. Anh, C. T., Cao, D. T., & Ngan, L. T. Q. (2025). Preparation of Colloidal Silver Triangular Nanoplates and Their Application in SERS Detection of Trace Levels of Antibiotic Enrofloxacin. *Colloids and Interfaces*, *9*(3), 31.
46. Urbina, I., Herrera, L. J. M., Etcheverry, M. E., Villa, C., Sepúlveda, R. D. M., Garavaglia, L., ... & Tebaldi, M. C. (2025). Shape modification of silver nano triangles under light irradiation. *Photonics and Nanostructures-Fundamentals and Applications*, 101470.
47. Escorcia-Díaz, D., García-Mora, S., Rendón-Castrillón, L., Ramírez-Carmona, M., & Ocampo-López, C. (2023). Advancements in nanoparticle deposition techniques for diverse substrates: a review. *Nanomaterials*, *13*(18), 2586.
48. Badán, J. A., Navarrete-Astorga, E., Henriquez, R., Martin, F., Marotti, R. E., Ramos-Barrado, J. R., & Dalchiele, E. A. (2020). Optical properties of silver nanoparticles deposited onto silicon substrates by different soft-solution processing techniques. *Optical Materials*, *100*, 109651.
49. Thouti, E., Chander, N., Dutta, V., & Komarala, V. K. (2013). Optical properties of Ag nanoparticle layers deposited on silicon substrates. *Journal of Optics*, *15*(3), 035005.
50. Thirugnanasambandan, T., Pal, K., Abd Elkodous, M., Prasath, H., Kulasekarapandian, K., Ayeshamariam, A., & Jeevanandam, J. (2018). Aggrandize efficiency of ultra-thin silicon solar cell via topical clustering of silver nanoparticles. *Nano-Structures & Nano-Objects*, *16*, 224-233.
51. Al-Masoodi, A. H. H., Goh, B. T., Al-Masoodi, A. H., & Abd Majid, W. H. B. (2020). Deposition of Silver Nanoparticles on Indium Tin Oxide Substrates by Plasma-Assisted Hot-Filament Evaporation. In *Thin Films*. IntechOpen.
52. Polywka, A., Tückmantel, C., & Görrn, P. (2017). Light controlled assembly of silver nanoparticles. *Scientific Reports*, *7*(1), 45144.
53. Tian, X., Zhang, B., Song, L., Bao, J., Yang, J., Sun, L., ... & Song, C. (2025). New Trends in SERS Substrates With Micro-and Nanostructures: Materials, Substrates, Preparation, and Applications. *Battery Energy*, *4*(4), e70023.
54. Paul, T. C., Hagen, G. M., Pinchuk, A. O., & McNear, K. L. (2022). Optimization of laser deposited silver nanoparticle substrates for surface-enhanced raman spectroscopy. *Nanotechnology*, *33*(31), 315703.
55. Mikalkevičius, M., Khinevich, N., Tamulevičius, S., Tamulevičius, T., & Tamulevičienė, A. (2024). Templated silver nanoparticle deposition on laser-induced periodic surface structures for SERS sensing. *Surfaces and Interfaces*, *51*, 104603.
56. Zhao, X., Zhao, C., Wen, J., Zhang, Y., Zhang, F., Gao, R., ... & Wang, Y. (2025). Growth of Silver Nanosheets Induced by Laser Direct Writing Lithography and Its SERS Performance. *Surfaces and Interfaces*, 107214.
57. Gibertini, E., Gervasini, L. F., Albertazzi, J., Facchetti, L. M., Tommasini, M., Busini, V., & Magagnin, L. (2025). Reactive Aerosol Jet Printing of Ag Nanoparticles: A New Tool for SERS Substrate Preparation. *Coatings*, *15*(8), 900.
58. Zhou, X., Liu, S., Xiang, H., Li, X., Wang, C., Wu, Y., & Li, G. (2025). Three-dimensional SERS substrates: Architectures, hot spot engineering, and biosensing applications. *Biosensors*, *15*(9), 555.
59. Zhang, C., Chen, S., Jiang, Z., Shi, Z., Wang, J., & Du, L. (2021). Highly sensitive and reproducible SERS substrates based on ordered micropyramid array and silver nanoparticles. *ACS applied materials & interfaces*, *13*(24), 29222-29229.
60. Jin, R., Cao, Y., Mirkin, C. A., Kelly, K. L., Schatz, G. C., & Zheng, J. G. (2001). Photoinduced conversion of silver nanospheres to nanoprisms. *science*, *294*(5548), 1901-1903.
61. Jin, R., Charles Cao, Y., Hao, E., Métraux, G. S., Schatz, G. C., & Mirkin, C. A. (2003). Controlling anisotropic nanoparticle growth through plasmon excitation. *Nature*, *425*(6957), 487-490.
62. Yin, Z., He, H., Wang, Z., Fang, X., Xu, C., Luo, D., ... & Liu, Y. J. (2020). Facile in situ photochemical synthesis of silver nanoaggregates for surface-enhanced Raman scattering applications. *Nanomaterials*, *10*(4), 685.
63. Kosuda, K., Bingham, J., Wustholz, K., & Van Duyne, R. (2010). Nanostructures and surfaceenhanced Raman spectroscopy. *Handbook of Nanoscale Optics and Electronics*, *309*.
64. Chaumet, P. C. (2022). The discrete dipole approximation: A review. *Mathematics*, *10*(17), 3049.
65. Johnson, P. B., & Christy, R. W. (1972). Optical constants of the noble metals. Physical Review B, 6(12), 4370–4379.

66. Mendoza-Herrera, L. J., Urbina, I., Mojica-Sepúlveda, R. D., Etcheverry, M. E., Arce, V. B., & Tebaldi, M. C. (2026). Influence of incident light properties on the formation of silver nanotriangles from spherical nanoparticles. *Photonics and Nanostructures-Fundamentals and Applications*, 101557.
67. Huang B., Miao L., Li J., Xie Z., Wang Y., Chai J., Zhai Y. (2022). Identification of plasmon-driven nanoparticle-coalescence-dominated growth of gold nanoplates through nanopore sensing. *Nat. Commun*., 13. 1402.
68. Jin, R., Charles Cao, Y., Hao, E., Métraux, G. S., Schatz, G. C., & Mirkin, C. A. (2003). Controlling anisotropic nanoparticle growth through plasmon excitation. *Nature*, *425*(6957), 487-490.
69. Kavitha, C., Bramhaiah, K., John, N. S., & Aggarwal, S. (2017). Improved surface-enhanced Raman and catalytic activities of reduced graphene oxide–osmium hybrid nano thin films. *Royal Society open science*, *4*(9), 170353.
70. Ayhan, M. E., Kalita, G., Kondo, M., & Tanemura, M. (2014). Photoresponsivity of silver nanoparticles decorated graphene–silicon Schottky junction. *RSC Advances*, *4*(51), 26866-26871.
71. Frydendahl, C., Indukuri, S. R. K. C., Devidas, T. R., Han, Z., Mazurski, N., Watanabe, K., ... & Levy, U. (2024). hBN-Encapsulated Graphene Coupled to a Plasmonic Metasurface via 1D Electrodes for Photodetection Applications. *Advanced Photonics Research*, *5*(4), 2300192.

Bulavinets, T., Kachurak, Y., Shepida, M., Lapinski, M., Lepek, A., Helzhynskyy, I., Ivaniuk, Kh., Stakhira, P., and Yaremchuk, I. (2026). Dispersion- and Diffraction-Induced Evolution of Longitudinal Polarization Forces in Ultrashort Laser Pulses. *Ukrainian Journal of Physical Optics*, *27*(4), 04178 – 04192. doi: 10.3116/16091833/Ukr.J.Phys.Opt.2026.04178

Анотація. *Реалізовано та порівняно два методи формування плазмонних шарів наночастинок срібла (AgNP) на підкладках ITO/CuI з метою встановлення впливу способу формування на морфологію та оптичні властивості шару. У першому методі колоїд AgNP фотохімічно модифікують під дією світлодіодного випромінювання вибраних довжин хвиль, після чого модифіковані частинки переносять на підкладку методом крапельного осадження. Другий метод ґрунтується на лазерно-стимульованому фотовідновленні іонів срібла, що забезпечує безпосередній ріст AgNP in situ на поверхні підкладки. Опромінення стабілізованого цитратом колоїду сферичних AgNP зеленими та червоними світлодіодами спричиняє появу додаткових плазмонних смуг при 584 і 975 нм, а також при 710 і 1050 нм відповідно. Крапельне осадження модифікованих колоїдів на підкладки ITO/CuI дає змогу отримати покриття з різною морфологією: з великих частинок, організованих у ланцюжкові та сіткоподібні агрегати, а також із дрібних трикутних частинок. Застосування лазерно-індукованого синтезу AgNP безпосередньо на поверхні ITO/CuI забезпечує формування суцільного однорідного шару анізотропних пластинчастих наноструктур. Встановлено, що архітектуру шару визначає насамперед спосіб осадження, а не лише попередня обробка колоїду, причому найщільніші та найоднорідніші шари утворюються за лазерно-індукованого синтезу in situ. Можливість зміщення плазмонного резонансу в ближню інфрачервону область і формування щільних однорідних плазмонних шарів на прозорих струмопровідних підкладках робить метод лазерно-індукованого синтезу перспективним для підсилення локального електромагнітного поля.*

Ключові слова: *наночастинки срібла, фотомодифіковані колоїди, поглинання, підкладка.*